would be strengthened. Still, apart from the roughly one-sixth of the NEA population thought to be binary systems (*28*), measuring the strength of the Yarkovsky acceleration offers the only means of estimating the masses of sub-kilometer NEAs from Earth-based observations.

References and Notes

1. D. P. Rubincam, *J. Geophys. Res.* **100**, 1585 (1995).
2. D. P. Rubincam, *J. Geophys. Res.* **103**, 1725 (1998).
3. P. Farinella, D. Vokrouhlický, W. K. Hartmann, *Icarus* **132**, 378 (1998).
4. D. Vokrouhlický, *Astron. Astrophys.* **335**, 1093 (1998).
5. D. Vokrouhlický, *Astron. Astrophys.* **344**, 362 (1999).
6. W. F. Bottke, D. Vokrouhlický, D. P. Rubincam, M. Brož, in *Asteroids III*, W. F. Bottke Jr., A. Cellino, P. Paolicchi, R. P. Binzel, Eds. (Univ. Arizona Press, Tucson, AZ, 2003), pp. 395–408.
7. W. F. Bottke, D. P. Rubincam, J. A. Burns, *Icarus* **145**, 301 (2000).
8. P. Farinella, D. Vokrouhlický, *Science* **283**, 1507 (1999).
9. A. Morbidelli, D. Vokrouhlický, *Icarus* **163**, 120 (2003).
10. D. Vokrouhlický, P. Farinella, *Nature* **407**, 606 (2000).
11. W. F. Bottke, D. Vokrouhlický, M. Brož, D. Nesvorný, A. Morbidelli, *Science* **294**, 1693 (2001).
12. J. D. Giorgini *et al.*, *Science* **296**, 132 (2002).
13. D. P. Rubincam, *J. Geophys. Res.* **92**, 1287 (1987).
14. D. Vokrouhlický, A. Milani, S. R. Chesley, *Icarus* **148**, 118 (2000).
15. D. Vokrouhlický, S. R. Chesley, A. Milani, *Celest. Mech. Dyn. Astron.* **81**, 149 (2001).
16. D. K. Yeomans, S. J. Ostro, P. W. Chodas, *Astron. J.* **94**, 189 (1987).
17. S. J. Ostro *et al.*, *Bull. Am. Astron. Soc.* **23**, 1144 (1991).
18. R. S. Hudson *et al.*, *Icarus* **148**, 37 (2000).
19. Materials and methods are available as supporting material on *Science* Online.
20. The asteroid's mass and bulk density are related through the volume of the shape model, which is 7.79465×10^7 m^3 (*18*).
21. A. E. Wechsler, P. E. Glaser, A. D. Little, J. A. Fountain, in *Thermal Characteristics of the Moon*, J. W. Lucas, Ed. (MIT Press, Cambridge, MA, 1972), pp. 215–242.
22. A. W. Harris, J. S. V. Lagerros, in *Asteroids III*, W. F. Bottke Jr., A. Cellino, P. Paolicchi, R. P. Binzel, Eds. (Univ. Arizona Press, Tucson, AZ, 2003), pp. 205–218.
23. M. G. Langseth, E. M. Drake, D. Nathanson, J. A. Fountain, in *Thermal Characteristics of the Moon*, J. W. Lucas, Ed. (MIT Press, Cambridge, MA, 1972), pp. 169–204.
24. K. Yomogida, T. Matsui, *J. Geophys. Res.* **88**, 9513 (1983).
25. S. J. Bus, R. P. Binzel, *Icarus* **158**, 146 (2002).
26. G. J. Consolmagno, D. T. Britt, C. P. Stoll, *Meteorit. Planet. Sci.* **33**, 1221 (1998).
27. D. T. Britt, D. Yeomans, K. Housen, G. Consolmagno, in *Asteroids III*, W. F. Bottke Jr., A. Cellino, P. Paolicchi, R. P. Binzel, Eds. (Univ. Arizona Press, Tucson, AZ, 2003), pp. 485–500.
28. J. L. Margot *et al.*, *Science* **296,** 1445 (2002).
29. S. R. Chesley *et al.*, data not shown.

30. We thank V. Negrón and the technical staff of the Arecibo Observatory for help with the radar observations; G. Garrad, W. Owen Jr., and T. Spahr for providing precise optical astrometry of Golevka; and S. Hudson for providing his shape reconstruction software. This research was conducted in part at the Jet Propulsion Laboratory, California Institute of Technology under a contract with NASA. Additional support was provided by the Grant Agency of the Czech Republic. The Arecibo Observatory is part of the National Astronomy and Ionosphere Center, which is operated by Cornell University under a cooperative agreement with NSF and with support from NASA.

Supporting Online Material
www.sciencemag.org/cgi/content/full/302/5651/1739/DC1
Materials and Methods
Fig. S1
Table S1
References

12 September 2003; accepted 30 October 2003

Water Isotope Ratios D/H, $^{18}O/^{16}O$, $^{17}O/^{16}O$ in and out of Clouds Map Dehydration Pathways

Christopher R. Webster[1*] and Andrew J. Heymsfield[2]

Water isotope ratios have been measured by laser absorption spectroscopy in and out of cirrus clouds formed in situ and convectively generated in anvils over subtropical regions. Water vapor in the tropical and subtropical upper troposphere shows a wide range of isotopic depletion not observed previously. The range suggests that dehydration of upper tropospheric air occurs both by convective dehydration and by gradual dehydration mechanisms. Twenty-five percent of upper tropospheric water sampled is in ice particles whose isotopic signatures are used to identify those grown in situ from those lofted from below.

Tropospheric water vapor is the most important greenhouse gas and a key component of the climate system (*1*). In the upper troposphere (UT) and lower stratosphere (LS), water vapor, liquid clouds, and ice particles substantially affect the radiation balance, atmospheric circulation, and chemistry (*2*). Cirrus clouds in particular affect UT water ice and vapor content, which global climate models indicate have large effects on Earth's radiative balance (*3–5*), especially in the dry subtropical UT (*6*).

Understanding the sources and sinks of water in the UT and LS and the mechanism of stratospheric dehydration is one of the important remaining challenges in Earth science, because water vapor feedback mechanisms can increase ozone depletion (*7*) and lead to stratospheric cooling (*8*). A doubling in stratospheric humidity over the last half century has been reported (*9*), despite decreasing tropical tropopause temperatures (*10*).

The extent to which the humidity of air transported from the troposphere into the stratosphere is controlled by tropopause minimum temperatures, cloud microphysics and convection, and mixing of air between high and low latitudes is not fully understood. The water vapor content of air entering the LS [3 to 4.1 parts per million volume (ppmv) (*11*)] is lower than the ice saturation mixing ratio (~4.5 ppmv) that would be determined by freeze-drying at the global mean tropopause temperature. Although there is consensus that dehydration occurs principally in the tropical tropopause layer (TTL) [covering the altitude range from ~13 to 19 km (*12*, *13*)], two competing mechanisms have been proposed: "convective dehydration" and "gradual dehydration" (*13*). Convective dehydration results from rising air masses overshooting their level of neutral buoyancy (LNB) to become severely dehydrated (≤1 ppmv by condensation and fallout) before mixing (*14–18*) with moister air. In gradual dehydration (*13*, *19–21*), air detrains from convection near its LNB at the bottom of the TTL and becomes dehydrated during slow ascent through regions that have temperatures below the tropopause global average temperature. This "cold trap" region need not be the local tropopause for a sampled air parcel, because time scales for horizontal versus vertical transport allow air parcels to "visit" far away cold pools such as that of the tropical Western Pacific (*13*).

Water vapor has a long lifetime (*22*), has an observed seasonal cycle (*19*, *23*), and is a good tracer of atmospheric transport. Its stable isotopes, especially HDO and $H_2{}^{18}O$ compared with $H_2{}^{16}O$, suffer large fractionations in an air parcel [expressed as delta-D (δD) and delta-^{18}O ($\delta^{18}O$) (*24*), respectively] as a result of condensation and sedimentation (*25*). Since the first tropospheric (*26*) and stratospheric (*27*) HDO measurements, subsequent studies (*28–33*) have recognized that water isotope fractionation is, in principle, a sensitive tracer for diagnosing transport and dehydration mechanisms.

Gradual dehydration is expected to follow Rayleigh distillation (*34*) in which all condensate is removed during adiabatic cooling. In this case, the vertical profile of δD for atmospheric water vapor is expected to begin at ~–86 per mil (‰) above the ocean [standard mean ocean water (SMOW) is 0‰ (*35*)] and reduce monotonically to ~–950‰ at the coldest tropopause. Few in situ measurements exist, particularly in tropical regions. Before the work presented here, such low values were usually not observed [except –837 ± 100‰ (*36*) in the polar vortex, and –810 ± 213‰ in the UT over Texas (*37*)]. At mid- and low-latitudes, UT values down to –670‰ have been reported (*38*).

[1]Earth and Space Sciences Division, Jet Propulsion Laboratory (JPL), California Institute of Technology, Pasadena, CA 91109, USA. [2]National Center for Atmospheric Research (NCAR), Boulder, CO 80301, USA.

*To whom correspondence should be addressed. E-mail: chris.r.webster@jpl.nasa.gov

The TTL region (*39*) is the best region for discriminating between dehydration mechanisms, because air passes through the TTL to enter the LS (fig. S1). From ATMOS stratospheric data that lacked ice observations, Moyer *et al.* (*30*) speculated that "ice lofting" (*15*) was responsible for the observed relative enrichment of stratospheric water vapor to δD of –670‰. Extending this same data set down into the UT, Kuang *et al.* (*40*) reported a near-constant value of δD = –648 ± 40‰ for water vapor from the tropical tropopause at 16.5 km down to ~13 km, a result reproduced by modeling (*41*) based on dehydration by convective processes.

For the Cirrus Regional Study of Tropical Anvils and Cirrus Layers Florida Area Cirrus Experiment [CRYSTAL-FACE, or C-F (*24*)] water isotopes were measured on the WB-57 aircraft by the Aircraft Laser Infrared Absorption Spectrometer (ALIAS) (*42*), a high-resolution tunable laser absorption spectrometer (*24*) that samples total water content of the atmosphere with an isokinetic, heated inlet. Calibration is discussed elsewhere (table S2). Water isotope mixing ratios were recorded on nine flights from 7 through 29 July 2002, and $H_2{}^{17}O$ data were recorded (*24*) only on 16 and 28 July. In Fig. 1, we present all the data with climb out values removed (*24*). As a rule, δD and $\delta^{18}O$ values show poor correlation with pressure and temperature, but tighter correlation with total water amount (figs. S3 and S4). We distinguish data associated with clouds by the difference between the total water (vapor, liquid, ice) mixing ratio, $(H_2O)_{tot}$, and the vapor-only mixing ratio, $(H_2O)_{vap}$, both measured during flights by the Harvard University instrument (*43*). The percentage of ice contributing to the measured isotope ratio is calculated by $[((H_2O)_{tot} - (H_2O)_{vap})/(H_2O)_{tot}] \times 100\%$. Our ability to identify ice crystals in the vicinity of the tropopause is determined by the above criterion and supporting simultaneous observations (*43*) (table S1) that include measurements from particle size spectrometers, cloud radar, ground radar daily mapping cirrus overpass, and detailed flight reports (*24*).

Most flights were in subtropical air near convective systems. A subset of data in the TTL region is selected according to three qualifying criteria: altitude between 13 and 17 km, potential temperature (*43*) >355 K, and the NOy/O_3 ratio $\times 10^{-3} < 2.0$, where $NOy = NO + NO_2 + HNO_3$ (*44*). All nine flights have contributing points to Fig. 2, especially the southern flights (9 and 26 July) that reached latitudes as low as 12° to 13°N off the east coast of Nicaragua, with tropopause heights varying from 13.9 to 15.5 km (*43*). Near the southern end of the 9 July flight, cold (–72°C) tropical cirrus was sampled (Fig. 3A). Two strong cloud layers were observed (~120 mbar, ~15 km, 16°N latitude) that had originated in the lower troposphere as identified from low O_3 and high CO values (*43*). The ER-2 aircraft cloud radar flying directly overhead confirmed that the cloud layers were deep-convectively generated (*24*), consistent with the observed high δD and $\delta^{18}O$ values (~0‰) during these encounters, compared with the low values (–600‰, –150‰) of the surrounding water vapor, indicating that these particles were lofted from below. In contrast, Fig. 3B shows thin (~2 km) subvisual cirrus clouds sampled on 13 July above and below a very cold

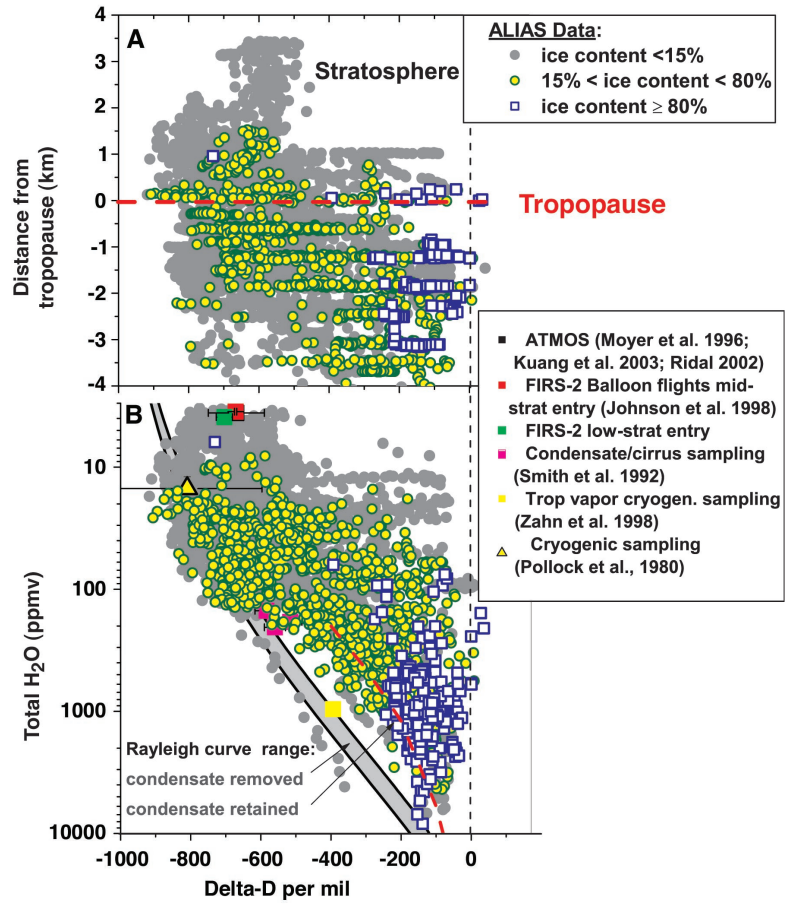

Fig. 1. δD intercomparison using unfiltered data (20 s averaged) from all nine flights versus distance from the tropopause (**A**) and versus total water (**B**). Tropopause location is from microwave temperature profiler (MTP) instrument (*43*) that identifies the thermal tropopause. The ATMOS (*30*, *31*, *40*) and FIRS-2 (*17*, *50*) stratospheric data lie on top of each other. Tropospheric data are included (*37*, *38*, *51*). The Rayleigh curves are from (*17*), and the retained condensate curve is from (*30*). A similar plot is obtained for $\delta^{18}O$ data.

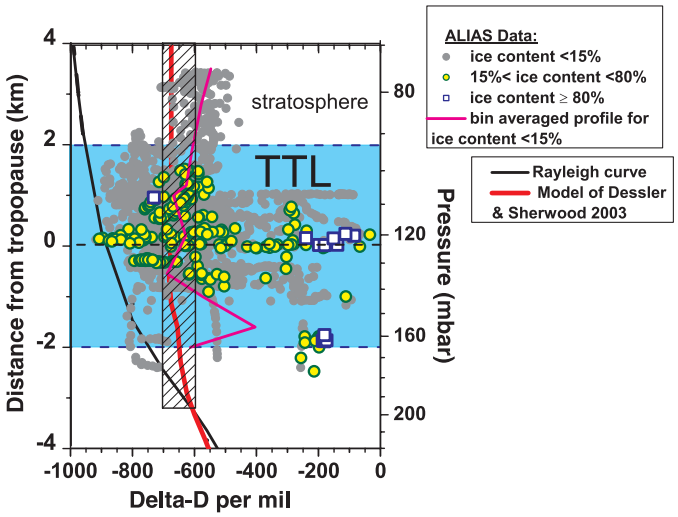

Fig. 2. Observations in the TTL compared with model calculations (*41*) that used δD_{ice} = –565‰. The dashed box represents ATMOS data of Kuang *et al.* (*40*). Mean tropopause level is 14.4 ± 0.5 km (*43*).

(195 K) tropopause near 14.8 km. Persistent and growing contrails and measurements (*43*) of ice supersaturation signified the presence of an environment suitable for in situ formation and growth of ice particles. Despite the relatively large change in total water mixing ratio, measured δD and $\delta^{18}O$ during transit through the cirrus showed little, if any, change (Fig. 3B). The thin cirrus carries an isotopic signature (up to 60% is ice) of its surrounding water vapor and, therefore, was not residual, lofted ice, but was formed in situ in air previously dehydrated.

For weather prediction and radiative transfer models, it is important to reliably parameterize ice particle size distributions (PSD) that have a large impact on convective cloud dynamics, notably hurricane dynamics. Small particles dominate cold cirrus clouds formed in situ, whereas large particles formed lower down at warmer temperatures are often lifted through deep convection into the UT to produce anvil cirrus (*45*). We have used PSDs (0.3 μm to ~3 mm) (*24*, *46*) to determine the slope λ of the change in particle concentration per unit change of size. For most data, λ values versus temperature (Fig. 3C) show a wide range, but a clear signal emerges when data are segregated by their isotopic content. Large λ values (>100 cm^{-1}) represent primarily in situ small particle generation, with δD ≤−150‰. Small λ values (<50 cm^{-1}) suggest large near-surface condensate, transported

Table 1. Lower stratospheric data (O_3 > 250 ppbv for ALIAS data) (*24*).

Data	Mean value (‰) ± 1σ	Range (min. to max.)	References
δD ALIAS	−635 ± 92	−460 to −870	This work
δD FIRS-2	−679 ± 20		(*50*)
δD ATMOS	−631 ± 80, −670 ± 80		(*29*, *30*)
δD Far IR	−560 ± 80		(*52*)
δD Cryogenic	−450 ± 100		(*37*)
$\delta^{18}O$ ALIAS	−248 ± 35	−119 to −292	This work
$\delta^{18}O$ FIRS-2	−128 ± 31		(*50*)

Table 2. UT data (top 3 km) values for "vapor" (<15% ice) and "ice" (>80% ice).

Data	No. points		Mean value (‰) ± 1 σ		Range (min. to max.)	
	Vapor	Ice	Vapor	Ice	Vapor	Ice
δD	3366	154	−600 ± 180	−130 ± 83	−918 to 9	−731 to 36
$\delta^{18}O$	3366	154	−179 ± 72	−42 ± 51	−292 to 88	−284 to 70
$\delta^{17}O$	917	53	−6 ± 30	−39 ± 23	−123 to 167	−75 to 3
Total H_2O (ppmv)	3544	154	78 ± 324	915 ± 554	3.3 to 6382	6 to 2508

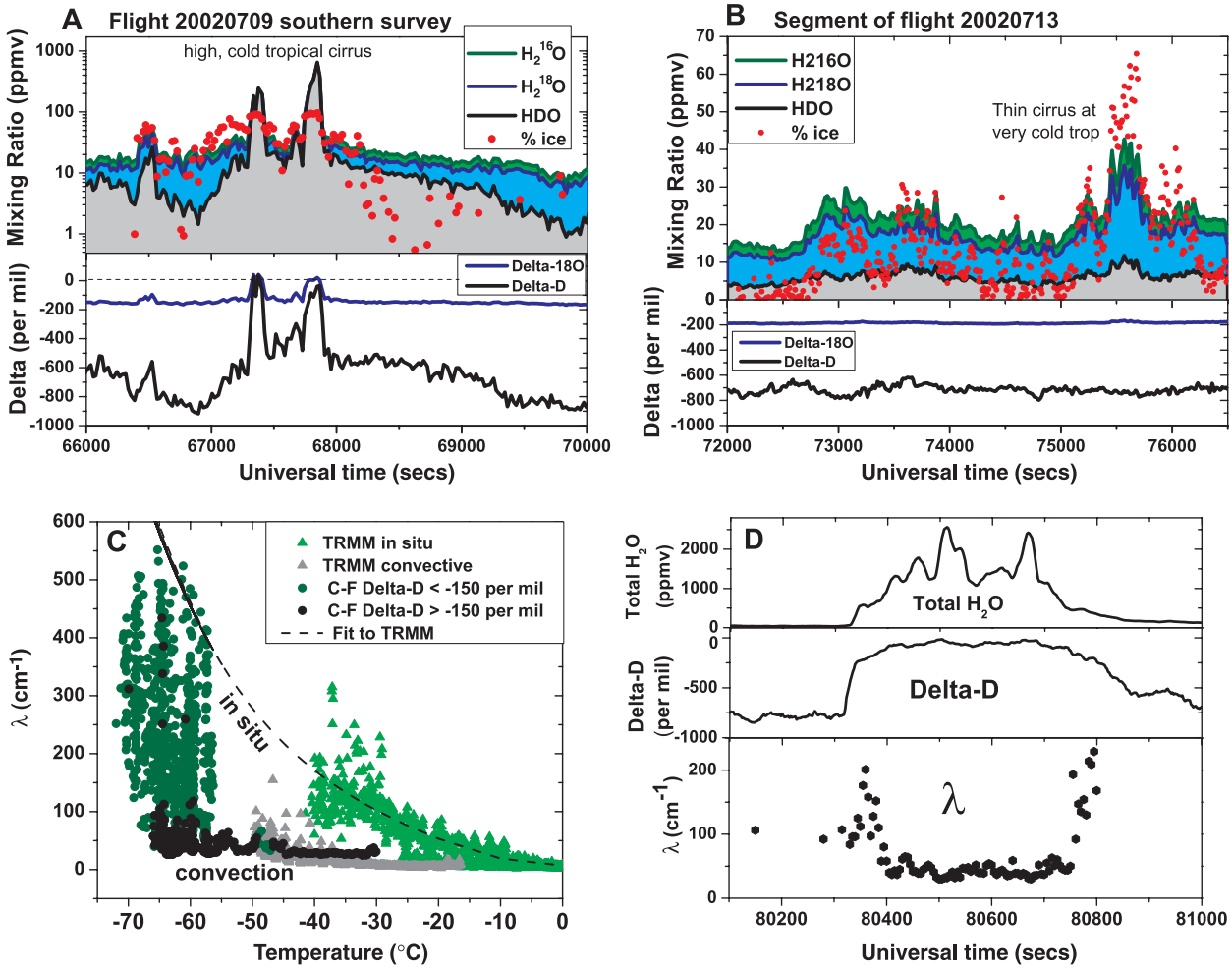

Fig. 3. Cirrus observations. Mixing ratios of HDO and $H_2{}^{18}O$ are normalized to equal that of $H_2{}^{16}O$ if SMOW (*24*). (**A**) The southern end of the 9 July flight showing cirrus encounters with high ice content. (**B**) Thin cirrus at the tropopause. (**C**) Lambda (cm^{-1}) versus air temperature for 11, 26, and 28 July. TRMM data (*47*) identified as in situ or convective and C-F data binned as shown. (**D**) Total water, δD, lambda values for 28 July flight crossing region of convective updraft whose core contained 2600 ppm H_2O.

to upper levels by deep convection, with corresponding $\delta D \leq -150‰$. Convection evidently generates appreciably lower values (than in situ) of λ at a given temperature in the UT, as also found in measurements (*47*) from a tropical convection case. Figure 3D shows λ values changing from ~100 cm^{-1} outside to ~40 cm^{-1} inside the core region of a convective system (fig. S5), with a high λ transition at the core edge which suggests that air entrained from the upper levels of the storm was carried downward and then into the updraft (*48*). Large particles transported up to high altitudes (Fig. 3D) can play a role in the desiccation of the UT through diffusional growth and subsequent transport of moisture downward to lower altitudes.

Stratospheric data are identified and selected using simultaneously measured ozone values (*43*) that exceed 250 parts per billion volume (ppbv) (Table 1, table S1). Our mean stratospheric value of δD agrees well with those of ATMOS and FIRS-2, but unlike these remote sensing measurements shows a wide range of values. Our mean value for $\delta\,^{18}O$ is significantly higher than that of FIRS-2.

In the lower troposphere, we attribute the observed (Fig. 1) departure from the Rayleigh curve (*24*) for both vapor and condensate to conditions prevailing during the mission, namely deep or strong convection events for which the gradual ascent Rayleigh result is not expected. In the UT, our data (Table 2) show that (i) convective processes loft to within 3 km of the tropopause ice crystals that are isotopically enriched (mean $\delta D_{ice} = -130‰$; mean $\delta^{18}O_{ice} = -42‰$); and (ii) this region also contains water vapor with a wide range of delta values (Fig. 2, Table 2).

Next, we assessed the extent to which lofted ice (*24*) contributes to the hydration of the UT over Florida. From the sum of ice and vapor contributions to total water, we calculate that the UT region sampled (top 3 km) had ~25% of its total water mixing ratio in ice. Locally, ice mixing ratios can be orders of magnitude higher than that of the vapor (Fig. 3A). Although, in supersaturated air, lofted ice will not be able to vaporize and contribute to hydrating the UT, analysis of our UT data set shows that the environment for evaporation exists (*49*). Regarding stratospheric air, if 22% of the UT water vapor mixing ratio came from evaporation of ice ($\delta D = -130‰$, $\delta^{18}O = -42‰$), then mixing with 78% of water vapor (e.g., with $\delta D = -800‰$, $\delta^{18}O = -270‰$) from gradual ascent would produce a value ($\delta D = -653‰$, $\delta^{18}O = -220‰$) close to that observed in the LS.

δD measurements in the TTL (Fig. 2) also show that ice with a wide range of deuterium content (δD ~0 to –900‰) is lofted into the lower half of the TTL, right up to the tropopause itself. Water vapor is also seen to show a wide range in isotopic values. At the upper end of the TTL, a narrower range of δD (mean ~–620‰) is seen entering the stratosphere. This value is very close to the mean value of –626‰ observed for all TTL data of Fig. 2, both values significantly lower than the mean value observed (–194‰) for ice in the TTL.

Modeling studies (*41*) that champion convective dehydration are unable to reproduce our observed variability in fractionation but are able to reproduce the "constant δD" profile of ATMOS (*40*) throughout the TTL no matter what values are chosen for either the retained ice/vapor ratio or the isotopic composition of ice. This model reproduces the ATMOS profile exactly by assuming a mean $\delta D_{ice} = -565‰$, different from our directly measured TTL value of –194‰. Unlike our study, ATMOS data do not show a range of values because of their coarse resolution (2 km vertical, 200 km horizontal). If we degrade our in situ data, binning with altitude and averaging, a near-constant profile (Fig. 2) can be produced.

In addition to the variability, an important difference between our data and that of ATMOS is our observation of many data points near the Rayleigh curve, a result that cannot be reproduced in the convective model (*41*), but one expected from gradual ascent with condensation. Indeed, it is tempting to assign data beyond the Rayleigh limit (Fig. 1) as evidence that these air parcels had previously seen temperatures below their local temperatures, consistent with the concept of cold pool visitation (*13*) or entrainment of dry air from above.

Our data provide direct evidence of the role of ice lofting in establishing the water content of the UT and show that the stratospheric values of δD and $\delta^{18}O$ result from the mixing within the TTL of air with a wide range of isotopic values. Air transported into the stratosphere through the TTL is, therefore, dehydrated through a mixture of convective dehydration and dehydration by condensation accompanying gradual ascent.

References and Notes

1. D. L. Hartmann, *Science* **295**, 811 (2002).
2. S. Solomon, *Rev. Geophys.* **37**, 275 (1999).
3. K. P. Shine, A. Sinha, *Nature* **354**, 382 (1991).
4. V. Ramanathan, W. Collins, *Nature* **351**, 27 (1991).
5. K.-N. Liou *et al.*, *Mon. Weather Rev.* **114**, 1167 (1986).
6. D.L. Hartmann, J. R. Holton, Q. Fu, *Geophys. Res. Lett.* **28**, 1969 (2001).
7. D. B. Kirk-Davidoff, E. J. Hintsa, J. G. Anderson, D. Keith, *Nature* **402**, 399 (1999).
8. P. M. Forster, K. P. Shine, *Geophys. Res. Lett.* **29** (no. 6), 10.1029/2001GL013909 (2002).
9. K. H. Rosenlof *et al.*, *J. Geophys. Res.* **28**, 1195 (2001).
10. W. J. Randel, F. Wu, D. J. Gaffen, *J. Geophys. Res.* **105**, 15509 (2000).
11. *Stratospheric Processes and their Role in Climate (SPARC) Assessment of UT/LS Water Vapour*, WCRP-113, WMO/TD-No.1043 (World Meteorological Organization, Geneva, 2000).
12. S. C. Sherwood, A. E. Dessler, *Geophys. Res. Lett.* **27**, 2513 (2000).
13. J. R. Holton, A. Gettelman, *Geophys. Res. Lett.* **28**, 2799 (2001).
14. H. S. Johnston, S. Solomon, *J. Geophys. Res.* **84**, 3155 (1979).
15. E. F. Danielsen, *Geophys. Res. Lett.* **9**, 605 (1982).
16. S. C. Sherwood, A. E. Dessler, *J. Atmos. Sci.* **58**, 765 (2001).
17. D. G. Johnson, K. W. Jucks, W. A. Traub, K. V. Chance, *J. Geophys. Res.* **106**, 12219 (2001).
18. S. C. Sherwood, *Geophys. Res. Lett.* **27**, 677 (2000).
19. A. W. Brewer, *Q. J. R. Meteorol. Soc.* **75**, 351 (1949).
20. R. E. Newell, S. Gould-Stewart, *J. Atmos. Sci.* **38**, 2789 (1981).
21. B. E. Potter, J. R. Holton, *J. Atmos. Sci.* **52**, 1034 (1995).
22. G. Brasseur, S. Solomon, *Aeronomy of the Middle Atmosphere* (D. Reidel Publishing Co., Dordrecht, Holland, ed. 2, 1985).
23. P. W. Mote *et al.*, *J. Geophys. Res.* **101**, 3986 (1996).
24. Materials and Methods are available as supporting material on *Science* Online.
25. J. A. Kaye, *Rev. Geophys.* **25**, 1609 (1987).
26. D. H. Ehhalt, *Tech. Note TN/STR 100* (NCAR, Boulder, CO, 1974).
27. T. G. Scholtz, D. H. Ehhalt, L. E. Heidt, E. A. Martell, *J. Geophys. Res.* **75**, 3049 (1970).
28. J. A. Kaye, *J. Atmos. Chem.* **10**, 39 (1990).
29. C. P. Rinsland *et al.*, *J. Geophys. Res.* **96**, 1057 (1991).
30. E. J. Moyer, F. W. Irion, Y. L. Yung, M. R. Gunson, *Geophys. Res. Lett.* **23**, 2385 (1996).
31. M. Ridal, A. Jonsson, M. Werner, D. P. Murtagh, *J. Geophys. Res.* **106**, 32283 (2001).
32. D. W. Keith, *J. Geophys. Res.* **105**, 15167 (2000).
33. S. D. Gedzelman, *Tellus* **40B**, 134 (1988).
34. R. E. Criss, *Principles of Stable Isotope Distribution* (Oxford Univ. Press, New York, 1999).
35. H. Craig, *Science* **133**, 1833 (1961).
36. M. Stowasser *et al.*, *J. Geophys. Res.* **104**, 19213 (1999).
37. W. Pollock, L. E. Heidt, R. Lueb, D. H. Ehhalt, *J. Geophys. Res.* **85**, 5555 (1980).
38. R. B. Smith, *J. Atmos. Sci.* **49**, 2041 (1992).
39. E. J. Highwood, B. J. Hoskins, *Q. J. R. Meteor. Soc.* **124**, 1579 (1998).
40. Z. Kuang, G. C. Toon, P. O. Wennberg, Y. L. Yung, *Geophys. Res. Lett.* **30**, 25 (2003).
41. A. E. Dessler, S. C. Sherwood, *Atmos. Chem Phys. Discuss.* **3**, 44-89-4513 (2003).
42. C. R. Webster, R. D. May, C. A. Trimble, R. G. Chave, J. Kendall, *Appl. Optics* **33**, 454 (1994).
43. For CRYSTAL-FACE mission and instruments, see the Web site at http://cloud1.arc.nasa.gov/crystalface.
44. D. W. Fahey *et al.* [*Geophys. Res. Lett.* **23**,1653 (1996)] describe the NOy/O_3 ratio in the LS. We note that TTL data with high NOy from lightning sources will be excluded.
45. C. A. Knight *et al.*, *J. Atmos. Sci.*, **38**, 2485 (1981).
46. See SOM Text for additional description of the CAPS instrument.
47. A. J. Heymsfield *et al.*, *J. Atmos. Sci.* **59**, 3 (2002).
48. I. R. Paluch, *J. Atmos. Sci.* **36**, 2467 (1979).
49. Of points identified as vapor, 55% have relative humidities (RH) <100% and 25% have RH <60% [JPL laser hygrometer data (*24*)]. In addition, for air of mixed ice and vapor (50% <ice content <100%), numerous points are found with RH values clearly below 100%.
50. D. G. Johnson, K. W. Jucks, W. A. Traub, K. V. Chance, *J. Geophys. Res.* **106**, 12211 (2001).
51. A. Zahn, V. Barth, K. Pfeilsticker, U. Platt, *J. Atmos. Chem.* **30**, 25 (1998).
52. B. M. Dinelli *et al.*, *Geophys. Res. Lett.* **24**, 2003 (1997).

53. The research here was carried out by the JPL, California Institute of Technology, under contract with NASA. We acknowledge NASA Code Y funding from the RSP and UARP programs. Field deployment of ALIAS was by JPL personnel C.W., G. Flesch, K. Modarress, J. Landeros, and R. Howe. Particle studies were done at NCAR (NASA-NSF W-10-024). We thank the C-F Project members M. Craig, E. Jensen, R. Friedl and M. Ross, M. Kurylo, and D. Anderson. A special thanks to E. Schneider, S. Feaster, S. Reagan, and B. Ehrenstrom, S. Baccus, B. Barnett, and S. Reagan. We also thank E. Weinstock, A. Banserner, D. Baumgardner, E. Richard, M. J. Mahoney, G. Heymsfield, and P. Bui for allowing us to use their measurements before publication, and thank C. Knight, A. Eldering, B. Herman, and our reviewers for valuable comments on the manuscript.

Supporting Online Material
www.sciencemag.org/cgi/content/full/302/5651/1742/DC1
Materials and Methods
SOM Text
Figs. S1 to S5
Tables S1 to S3

22 July 2003; accepted 29 October 2003